Global Biogeochemical Cycles

RESEARCH ARTICLE
10.1029/2020GB006569

Key Points:

- Advection and dust deposition are the main processes driving the surface gradient of dissolved aluminum in the subtropical North Atlantic
- Lesser Antilles erosion products are a possible source of dissolved aluminum to the western subtropical North Atlantic
- Dissolved-particle interactions play a major role in the dissolved aluminum distribution in the subtropical North Atlantic

Supporting Information:

Supporting Information may be found in the online version of this article.

Correspondence to:

L. Artigue,
lise.artigue@gmail.com

Citation:

Artigue, L., Wyatt, N. J., Lacan, F., Mahaffey, C., & Lohan, M. C. (2021). The importance of water mass transport and dissolved-particle interactions on the aluminum cycle in the subtropical North Atlantic. *Global Biogeochemical Cycles*, *35*, e2020GB006569. https://doi.org/10.1029/2020GB006569

Received 5 FEB 2020
Accepted 29 MAR 2021

Author Contributions:

Conceptualization: Lise Artigue, Neil J. Wyatt, François Lacan, Claire Mahaffey, Maeve C. Lohan
Data curation: Lise Artigue, Neil J. Wyatt
Formal analysis: Lise Artigue, François Lacan
Funding acquisition: Lise Artigue, François Lacan, Claire Mahaffey, Maeve C. Lohan
Investigation: Lise Artigue, Neil J. Wyatt, François Lacan, Claire Mahaffey, Maeve C. Lohan
Methodology: Lise Artigue, Neil J. Wyatt, François Lacan, Maeve C. Lohan
Project Administration: François Lacan, Claire Mahaffey, Maeve C. Lohan

The Importance of Water Mass Transport and Dissolved-Particle Interactions on the Aluminum Cycle in the Subtropical North Atlantic

Lise Artigue[1], Neil J. Wyatt[2], François Lacan[1], Claire Mahaffey[3], and Maeve C. Lohan[2]

[1]LEGOS, University of Toulouse, CNRS, CNES, IRD, UPS, Toulouse, France, [2]Ocean and Earth Science, University of Southampton, National Oceanographic Center, Southampton, UK, [3]Department of Earth, Ocean and Ecological Sciences, University of Liverpool, Liverpool, UK

Abstract New dissolved aluminum (dAl) data from the 2017 GEOTRACES process study GApr08 along 22°N in the subtropical North Atlantic are presented. They show an east to west increase in dAl concentration in the surface waters. Simulation of these data with a 1D advection-dust deposition revealed that, (a) advection and dust dissolution are equally important dAl sources, (b) scavenging plays a minor role compared to advection in dAl removal, and (c) in addition to dust dissolution, another dAl source is required at the westernmost stations to fully explain our observations. We attribute this additional source to the dissolution of erosion products delivered to the western subtropical North Atlantic by the Lesser Antilles. For waters deeper than ~200–300 m, an optimum multi-parameter analysis allowed to separate the component of the dAl signal derived from water mass transport from its biogeochemical component. This revealed, (a) a major role played by water mass transport, (b) a net dAl removal between 200 and 800 m, attributed to scavenging at the subtropical North Atlantic scale, and (c) internal dAl inputs between 800 m and the seafloor, attributed to reversible scavenging. While the dAl oceanic distribution is usually considered to be dominated by the atmospheric dust input and removal by particle scavenging, this study highlights the important role played by advection, and the need to explicitly take this into account in order to quantitatively reveal the impact of external sources and dissolved-particulate interactions on the Al cycle in the North Atlantic Ocean.

1. Introduction

Aluminum (Al) is the third most abundant element in Earth's crust (8.15% by weight, Rudnick & Gao, 2014) and is widely used as a tracer for lithogenic materials to the oceans, particularly the delivery of atmospheric dust to the open ocean (Han et al., 2008; Measures & Vink, 2000; Measures et al., 2005). Knowledge of the distribution and concentration of Al therefore helps us to constrain the oceanic cycle of other crustal-derived elements, including those directly involved in primary production (e.g., iron). The cycling of Al in the marine environment has been hotly debated throughout the years (Measures et al., 2015). Initially, fluvial inputs had been considered as the major source of dissolved Al (dAl) to the surface ocean (Stoffyn & Mackenzie, 1982). It has been since shown that dAl is heavily scavenged in estuarine and coastal environments, and therefore, fluvial inputs constitute a negligible flux of dAl to the remote open ocean (Brown et al., 2010; Hydes & Liss, 1977; Mackin & Aller, 1984; Orians & Bruland, 1986). The dissolution of atmospheric aerosols is now considered to be the major source of dAl to open ocean surface waters (Jickells et al., 1994; Maring & Duce, 1987; Measures et al., 2005, 2010; Tria et al., 2007). At the sea floor, sediment resuspension also acts as a source of dAl, especially in regions with strong boundary currents and nepheloid layers (Middag et al., 2009, 2012; Middag, van Hulten, et al., 2015; Moran & Moore, 1991; van Hulten et al., 2013). Finally, hydrothermal vents can provide significant dAl inputs that could be transported over local to basin scales in the abyssal ocean (Hydes et al., 1986; Lupton et al., 1993; Measures et al., 2015; Resing et al., 2015). Dissolved Al is removed from the water column by particle scavenging, that is, surface adsorption and particle settling (Hydes, 1979; Orians & Bruland, 1986; Stoffyn & Mackenzie, 1982), and can be removed by incorporation into diatomaceous material in some ocean regions (Gehlen et al., 2002; Hydes et al., 1988; Middag et al., 2009; Middag, van Hulten, et al., 2015). Model results suggested that during sinking, desorption and dissolution of particulate Al (pAl) constitute a source of dAl to the water column (van Hulten et al., 2013).

Resources: François Lacan, Maeve C. Lohan
Software: Lise Artigue, François Lacan
Supervision: François Lacan, Maeve C. Lohan
Validation: Lise Artigue
Visualization: Lise Artigue, Neil J. Wyatt
Writing – original draft: Lise Artigue
Writing – review & editing: Lise Artigue, Neil J. Wyatt, François Lacan, Claire Mahaffey, Maeve C. Lohan

The present work provides a detailed study of the factors driving the distribution and concentration of dAl in the subtropical North Atlantic. To constrain the processes driving the observed east to west gradient in surface dAl, we utilized a 1D model that included both dust and advection as sources of dAl, and both advection and scavenging as sinks of dAl. In deeper waters, an extended optimum multi-parameter analysis (eOMPA, Artigue et al., 2020) is used to estimate how water mass transport and biogeochemical cycling (i.e., external inputs, dissolved/particulate interactions) impact the dAl distribution at the basin scale. In this study, the application of the surface model and the eOMPA provides new insights on the processes controlling the dAl distribution in the subtropical North Atlantic.

2. Materials and Methods

2.1. Sampling and Processing

Seawater samples were collected during the GEOTRACES process cruise (GApr08, Figure 1) in the sub-tropical North Atlantic along ~22°N, ~58°–31°W on-board the *R.R.S. James Cook*. This cruise departed Point-à-Pitre, Guadeloupe, on June 27, 2017, and ended in Santa Cruz, Tenerife, on August 12, 2017. Seawater samples were collected from seven full depth stations using 24 trace metal clean 10 L Teflon-coated Ocean Test Equipment (OTE) externally closing bottles and mounted on a titanium CTD rosette deployed on a Kevlar coated conducting wire. At each station a shallow (<700 m) and deep (>600 m) CTD cast was sampled resulting in seven high resolution, full depth vertical dAl profiles. Upon recovery, the OTE bottles were transferred into a class ISO 6 clean air container and pressurized with compressed air (1.7 bar) filtered in-line through a 0.2 μm PTFE filter capsule (Millex-FG 50, Millipore). All samples for trace metals were filtered through 0.2 μm membrane cartridge filters (Sartobran-300, Sartorious) into 125 mL low density polyethylene bottles (LDPE, Nalgene). Each sub-sample was acidified to pH 1.7 (0.024 M) with ultra-pure hydrochloric acid (HCl, UPA, Romil). In total, 201 samples were analyzed for dAl from the vertical profiles. Surface seawater samples (130 total) were collected underway using a towed fish positioned at approximately 5 m depth. Seawater was pumped from the fish into the trace metal clean container through acid–cleaned, braided PVC tubing connected to a Teflon diaphragm pump (Almatec A-15). Sub-samples were filtered in-line through a 0.8/0.2 μm polyethersulfone membrane filter capsule (Sartobran, Sartorius).

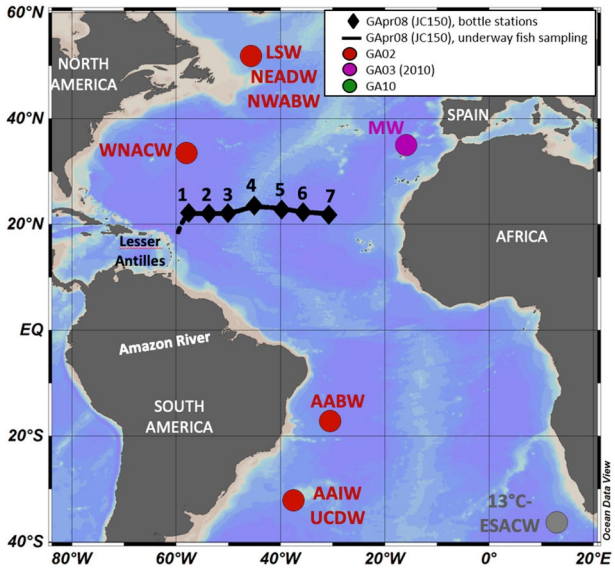

Figure 1. Cruise track of the GApr08 North Atlantic transect. Also shown are the locations where the extended optimum multiparameter analysis end-members of Artigue et al. (2020) were defined: West North Atlantic Central Water (WNACW), Antarctic Intermediate Water (AAIW), Upper Circumpolar Deep Water (UCDW), Labrador Sea Water (LSW), North East Atlantic Deep Water (NEADW), North West Atlantic Bottom Water (NWABW), Antarctic Bottom Water (AABW).

2.2. Dissolved Al Analysis

Samples were analyzed for dAl at the University of Southampton Waterfront Campus, National Oceanography Centre using the flow injection analysis (FIA) with fluorescence detection (Figure S1) based on the protocol of Resing and Measures (1994) and modified by Brown and Bruland (2008).

Briefly, the cation exchange resin Toyopeal-AF-Chelate 650 M (Tosohass) was preconditioned with a 0.1 M ammonium acetate solution (Romil, SpA) for 15 s. Seawater samples were buffered in-line to pH 5.75 using a 0.3 M ammonium acetate solution before dAl was preconcentrated onto the resin for 60 s at a flow rate of 1.5 ml/min. Dissolved Al was eluted from the resin using 0.1 M HCl (Romil, SpA) for 2.5 min, entering the reaction stream where it mixed with a lumogallion/ammonium acetate buffer solution. The resulting fluorescent lumogallion-Al complex formed as the reaction stream passed through a water bath set to 50 °C. The stream was then mixed with the nonionic surfactant 5% Brij-35 solution (Merck) to enhance the fluorescence quantum yield (Resing & Measures, 1994). Fluorescence was detected using a Shimadzu RF20Axs fluorometer with excitation and emission wavelengths set to 489 and 559 nm, respectively. Dissolved Al concentration was quantified by the method of standard addition (TraceCERT, Fluka Analytical, Al concentration of 0.037 mol/kg) on column cleaned (Chelex-100, Sigma-Aldrich) seawaters with a dAl concentration ranging from 0.893 nmol/kg to 2.891 nmol/kg. Except

when explicitly mentioned, all uncertainties presented in this paper will be expressed at a confidence level of 95% (e.g., two standard deviation of repeated measurement). Accuracy was quantified through repeated measurement of the SAFe S reference seawater yielding an average concentration of 1.75 ± 0.33 nmol/kg (n = 9), in good agreement with the consensus value of 1.67 ± 0.20 nmol/kg (www.geotraces.org). Measurements of the GSP and GSC reference seawater yielded concentrations of 1.32 ± 0.14 nmol/kg (n = 13) and 0.61 ± 0.16 nmol/kg (n = 13), respectively. Consensus values for the GSP and GSC dAl concentration are yet to be published. However, the GSP and GSC data confirmed the measurement precision. Surface water collected from the towed fish was used as an internal standard (fish sample 130) as its concentration was representative of that in most of our samples. Its repeated measurement yielded a dAl concentration of 15.29 ± 0.38 nmol/kg (n = 8). This corresponds to a relative precision of 2.5%, similar to the precision determined from triplicate analysis of each sample (<5%). The limit of detection (3x the standard deviation of the lowest standard) was 0.15 ± 0.22 nmol/kg (n = 60).

Possible dAl contamination due to batch-to-batch variability in the polypropylene (PP) caps of LDPE bottles has been previously reported (Brown & Bruland, 2008). This was investigated during this study following the protocol described by Brown and Bruland (2008). Ten acid-cleaned 125 mL LDPE bottles with PP caps were filled with 90 ml of column-cleaned and acidified (0.024 M HCl) seawater. Five bottles were placed upright and five inverted on their caps. All samples were measured before and after 1 week. We observed no significant increase in dAl in the upright bottles (0.22 ± 0.30 nmol/kg) but an increase in dAl in the inverted bottles (0.43 ± 0.39 nmol/kg). Although caps may be an important source of contamination in low dAl waters, the contamination represented only ~2% of the lowest concentration measured during this study.

3. Results

Along the section GApr08, dAl concentration ranged from 10 to 50 nmol/kg (Figures 2a and 2b). This is in good agreement with the range of dAl values previously reported for the North Atlantic (~5–50 nmol/kg, Barrett et al., 2015; Hydes, 1979; Measures et al., 1986, 2015; Menzel Barraqueta, Schlosser, et al., 2018; Middag, van Hulten, et al., 2015; Moran & Moore, 1991; Orians & Bruland, 1986).

Specifically, four main features are notable in the GApr08 dAl distributions (Figure 2). First, dAl in the upper 100 m displays a strong concentration gradient with values increasing westward from 13 to 49 nmol/kg between 31° and 58°W. This concentration gradient correlates well with that of the dissolved iron from the same study (Kunde et al., 2019). Second, a marked dAl minimum (<15 nmol/kg) was observed across the entire GApr08 zonal section between 700 and 1,500 m depth. Third, below this dAl minimum, dAl concentrations increase and stabilize at around 20 nmol/kg. Finally, elevated dAl concentrations to a maximum 33 nmol/kg were observed at station 4 at depths below 3,340 m associated with the Snakepit hydrothermal site.

Figure 3 compares the GApr08 dAl data with that of other North Atlantic section cruises. At 50 m (Figure 3a), the gradient from low dAl concentrations in the east to higher concentrations in the west during GApr08 is consistent with the basin scale distribution of dAl. West of the mid-Atlantic ridge (MAR), the GA03 section (Measures et al., 2015) displays higher dAl values than the GApr08. These discrepancies may be attributed to temporal variation (variable flows and/or dust deposition), and/or to the fact that the GA03 is located north of the GApr08. East of the MAR, where the GA03 crosses the GApr08, the dAl data are in good agreement. At 1,000 m depth (Figure 3b), the dAl minimum was visible across the subtropical North Atlantic with concentrations lower than ~15 nmol/kg. At 4,000 m depth (Figure 3c), elevated dAl concentrations (>20 nmol/kg) compared with intermediate depths were visible across the North Atlantic.

Figure 4 compares dAl profiles from the GApr08 stations 1, 6, and 7 with profiles from closely located stations previously occupied; the GApr08 station 1 with the GA02 station 29 (~234 km distance, Figure 4a), the GApr08 station 6 with the GA03 station 20 (crossover station, Figure 4b), and the GApr08 station 7 with the A16N station 90 (~288 km away, Figure 4c). In the west Atlantic (Figure 4a), there is an excellent agreement in the dAl profiles below 800 m (except for one data point at 1,000 m). In the upper 1,000 m, the dAl concentrations during both cruises are within the same range with differences likely due to a temporal variation in dAl supply. In the east Atlantic, the dAl profiles of the GApr08 and GA03 (Figure 4b) are offset in waters deeper than 1,000 m. Here, the GA03 dAl concentrations are higher than that of the GApr08 with the

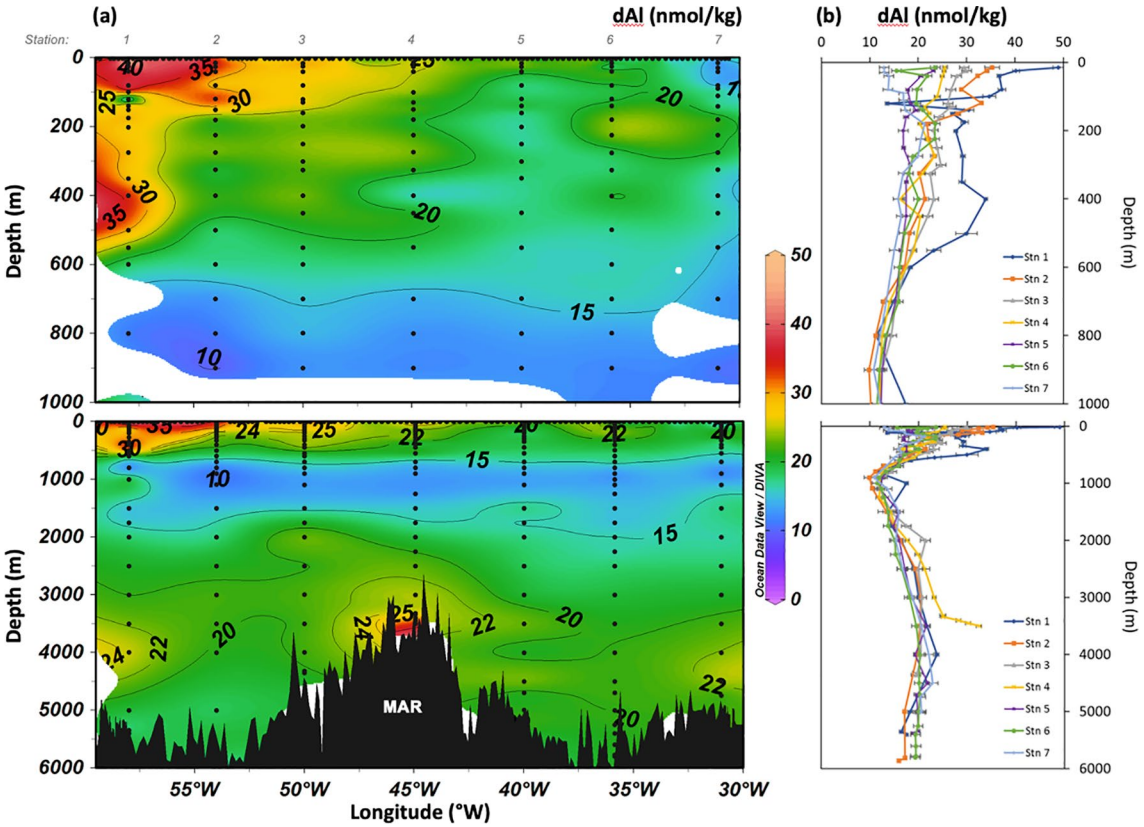

Figure 2. Dissolved aluminum concentrations presented (a) as color contour plots along the GApr08 section, including both bottle and towed fish data, and (b) by vertical profile for each of the seven stations. The upper figures show zooms on the upper 1,000 m, while the lower figures show the full depth range.

difference increasing with depth (i.e., 28% at 1,000 m to 42% at 5,800 m). A similar dAl concentration offset for waters deeper than 1,000 m was observed at the GA02/GA03 crossover station in the western Atlantic, the reason for which remains unresolved (Measures et al., 2015; Middag, Seferian, et al., 2015; Middag, van Hulten, et al., 2015), while the GApr08 and GA02 data are in close agreement for the western North Atlantic. At the easternmost stations (Figure 4c), the dAl profiles are similar in the upper 1,000 m (no A16 N data are available deeper than 1,000 m). Overall, in addition to the good agreement we obtained with the SAFe S reference standard, this inter-comparison provides great confidence in the data presented in this work.

4. Discussion

To interpret our results, the following discussion is organized in two main parts. First, we discuss the westward increase in surface dAl concentration using a model of advective transport, atmospheric sources, and scavenging. Second, we investigate the distribution of dAl in intermediate and deep waters using an eOMPA (Artigue et al., 2020) in order to determine if the dAl distribution is driven by water mass transport and/or biogeochemical processes.

4.1. dAl in Surface Waters

4.1.1. Modeling of the Westward Transport and Dust Deposition in Surface Waters

Surface dAl concentration in the upper 100 m increases westward along the GApr08. At 22°N, surface waters are transported westwards within the North Equatorial current (NEC; Arnault, 1987; Fieux, 2010; Richardson & Walsh, 1986), which likely impacts the surface dAl distributions. In addition, large quantities of dust, mainly derived from the North African deserts, are transported all year long across the subtropical North Atlantic (Prospero, 1996; Prospero & Carlson, 1972; Prospero et al., 2014). The dissolution of dust is

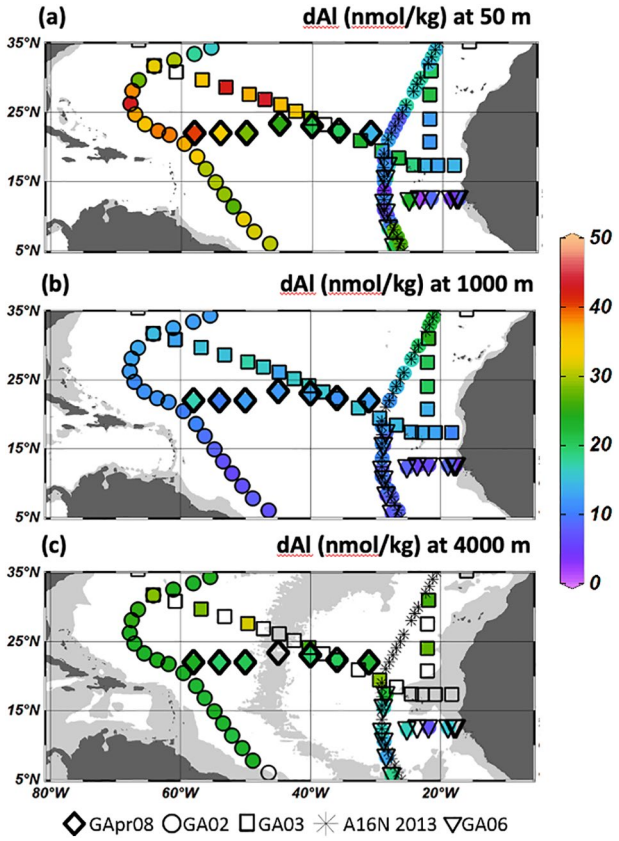

Figure 3. Depth horizon maps of dissolved aluminum (dAl) in the North Atlantic at (a) 50 m, (b) 1,000 m, and (c) 4,000 m. The data originate from several cruises: GApr08 (July 2017, this study); GA02 (May–July 2010, Middag, van Hulten, et al., 2015); GA03 (November–December 2011, Measures et al., 2015); A16 N (August–September 2013, Barrett et al., 2015); GA06 (March 2011, J. K. Klar, IDP 2017). Dissolved Al data was extracted from the GEOTRACES IDP 2017 (Schlitzer et al., 2018). Empty symbols indicate no dAl data were available.

considered to be the major source of dAl to open ocean surface waters (Maring & Duce, 1987). Along 22°N, the maximum winter mixed layer depth is estimated to be ~100 m, and therefore, the effect of dust dissolution is expected to impact this depth layer (de Boyer Montégut, 2004).

A simple model inspired from Roy-Barman and Jeandel (2016) is constructed below to simulate the evolution of the dAl concentration westward in the upper 100 m (x coordinate oriented west), considering the two processes of advection, and atmospheric deposition (Figure 5). Consequently, the model neglects in a first approximation all other processes, notably dAl removal onto particles (e.g., scavenging) or additional external sources. This will be discussed below.

Mass conservation implies that, within a volume (V), the dAl concentration (C) variation with time equals the net dAl flux into the volume:

$$\frac{d(CV)}{dt} = \underbrace{F_{\text{adv}}(x)\cdot dydz}_{F_{\text{in advection}}} - \underbrace{F_{\text{adv}}(x+dx)dydz}_{F_{\text{out advection}}} + \underbrace{F_{\text{dust}}(x)\cdot dxdy}_{F_{\text{in dust}}} \quad (1)$$

The volume V does not change with time, so we can divide Equation 1 by $dV = dxdydz$. After a first order Taylor expansion of the $F_{\text{out advection}}$ term, this leads to the following net flux equation:

$$\frac{dC}{dt} = -\frac{\partial F_{\text{adv}}(x)}{\partial x} + \frac{F_{\text{dust}}(x)}{dz} \quad (2)$$

Despite recent studies indicating that advection can be important for dAl distribution in the subtropical North Atlantic (Middag, van Hulten, et al., 2015), this process has been largely neglected and to our knowledge, not quantified while estimating the dust fluxes based on surface dAl measurement (Measures & Brown, 1996; Measures et al., 2005; Menzel Barraqueta, Klar, et al., 2018). However, in the case of strong horizontal gradients, such as dAl surface concentration along the GApr08, advection cannot be neglected. The quantity of dAl (dq) flowing through a surface ($dydz$) at a velocity (u), and during a time (dt) is as follows:

$$dq = C\cdot u\cdot dy\cdot dz\cdot dt \quad (3)$$

As the advected flux is the quantity of dAl (dq, refer to Equation 3) by unit of time (dt) and surface ($dydz$), this leads to the following advected flux:

$$F_{\text{adv}}(x) = \frac{dq\ /\ dt}{dy\cdot dz} = C(x)\cdot u \quad (4)$$

where u is the NEC velocity. The NEC velocity is modeled here as a constant (in time and space). The NEC velocity was established through a literature review (Arnault, 1987; Fieux, 2010; Richardson & Walsh, 1986), the results from a Lagrangian particle tracking experiment carried out along the GApr08 (Artigue et al., 2020), and finally, extracted from the global reanalysis GLORYS12V1 of the Copernicus Marine Environment Monitoring Service (CMEMS, Global_Reanalysis_Phy_001_030, http://marine.copernicus.eu/). We calculate a value of 2.8 cm/s as the mean current velocity for the upper 100 m, over the 3 years prior to the GApr08 for the latitude range 21°–24°N.

The total dust flux values used in this model were extracted from the Modern-Era Retrospective Analysis for Research and Applications version 2 (MERRA-2, Gelaro et al., 2017), using the database provided by the Global Modeling and Assimilation Office (GMAO, 2015, https://doi.org/10.5067/RZIK2TV7PP38). This atmospheric reanalysis data set developed by NASA includes both satellite data and conventional weather

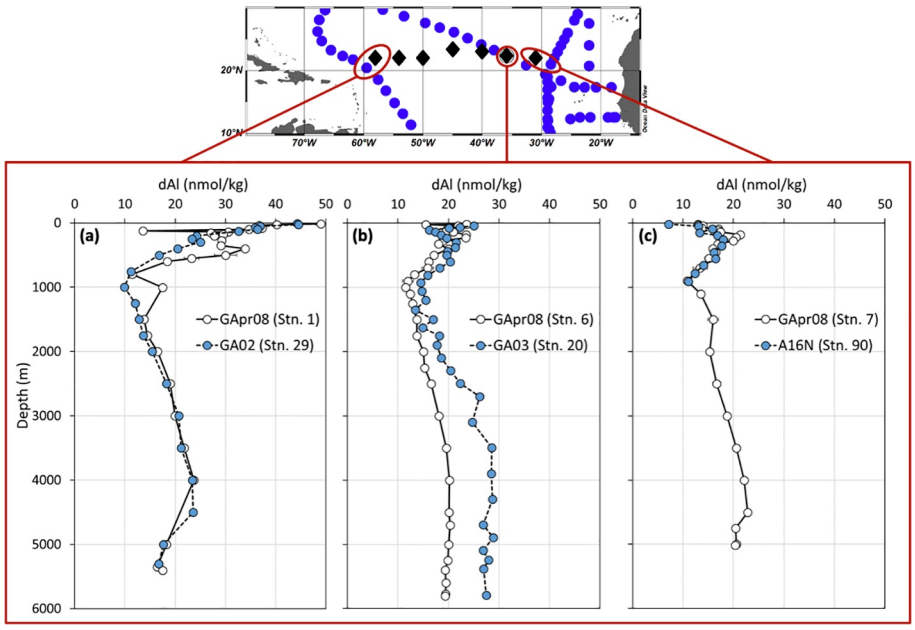

Figure 4. Dissolved aluminum profiles for three stations pairs in the subtropical North Atlantic Ocean: (a) GApr08 station 1 versus GA02 station 29 (Middag, van Hulten, et al., 2015); (b) GApr08 station 6 versus GA03 station 20 (Measures et al., 2015); (c) GApr08 station 7 versus A16N station 90 (Barrett et al., 2015).

observations (Gelaro et al., 2017). For the model, we determined the mean total (wet + dry) dust deposition for the 3 years prior to the GApr08 over the latitude range 21°–24°N, as for the NEC velocity. Modeled deposition to surface waters along the GApr08 (Figure 6) were consistent with the previous estimates for the subtropical North Atlantic (Jickells et al., 2005). A strong negative relationship was found between the dust flux and distance between station 7 and 1 that we modeled by linear regression ($ax + b$ in Equation 5).

The dust derived dAl flux, F_{dust} (mol m^{-2} day^{-1}), was obtained by multiplying the total dust flux ($ax + b$) with the Al concentration in the upper continental crust (D_{Al}) and the solubility of Al in aerosols (S_{Al}):

$$F_{\text{dust}}\left(x\right) = D_{\text{Al}} S_{\text{Al}} \cdot \left(ax + b\right) \tag{5}$$

with $a = -2.33$ E$-$12 kg m^{-3} day^{-1}, $b = 1.07$ E$-$5 kg m^{-2} day^{-1}, $D_{\text{Al}} = 3.02$ mol kg^{-1} (Rudnick & Gao, 2014), and $S_{\text{Al}} = 6.8\%$ (Baker et al., 2013).

Replacing the F_{adv} and F_{dust} terms defined in Equations 4 and 5, respectively, in Equation 2, leads to the net flux equation:

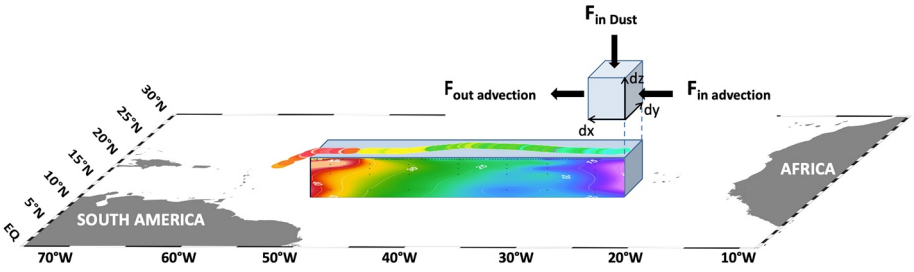

Figure 5. Schematic representation of how modeled advection, and dust deposition fluxes have been applied to the upper 100 m dissolved aluminum (dAl) data for GApr08. Input/output fluxes are designated by black arrows. The GApr08 upper 100 m dAl section as well as the towed fish dAl data are displayed on the map.

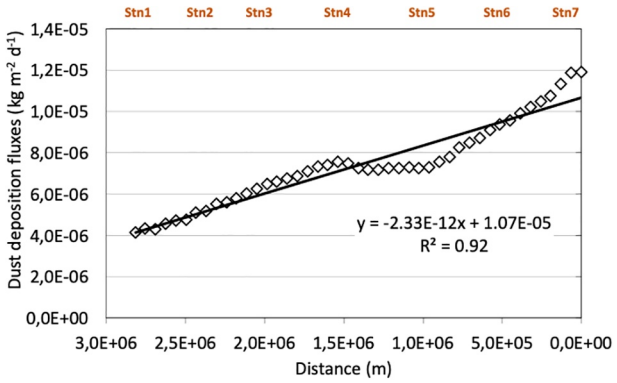

Figure 6. Mean total (wet + dry) dust deposition (white diamonds) for the latitude range 21°–24°N over 3 years prior to GApr08 (July 1, 2014–June 30, 2017) extracted from the Modern-Era Retrospective Analysis for Research and Applications version 2 (MERRA-2, Gelaro et al., 2017). The *x*-axis denotes the distance between station 7 ($x = 0$ m) and station 1 ($x = 2.82$ E 6 m). The linear regression line (black line), its equation and regression number are displayed.

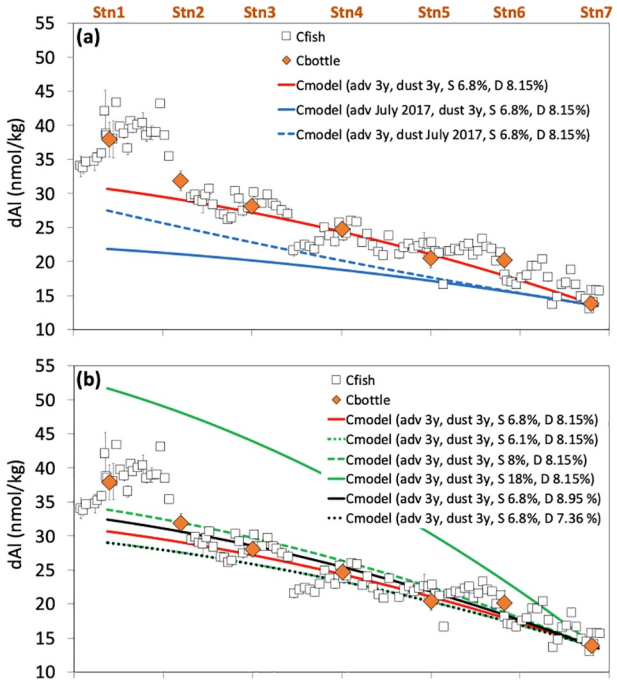

Figure 7. Measured versus modeled dissolved aluminum (dAl) distribution in the upper 100 m along GApr08. (a and b) Modeled dAl distribution from advection and dust deposition (C_{model}, red line) compared with measured dAl from the bottles (average dAl bottle value calculated by integration over the upper 100 m, $C_{bottles}$, orange diamonds) and from the towed fish (C_{fish}, white squares). The bottle and towed fish data are plotted with their respective uncertainties: 2 standard deviation of triplicate peaks for fish values and an estimate of the 95% error interval for the average bottle values. Different parameter settings for C_{model} were tested by variation of (a) North Equatorial current velocity and dust flux (blue solid and dashed lines, respectively), and (b) aluminum solubility (green solid and dashed lines) and the aluminum content of dust (black solid and dotted lines).

$$\frac{dC}{dt} = -u\frac{dC(x)}{dx} + \frac{D_{Al}S_{Al}(ax+b)}{dz} \quad (6)$$

We assumed that the dAl concentration was in a steady state, and that the height of the box was fixed at $dz = h = 100$ m. Using these assumptions and after integration of Equation 6, we obtained the following polynomial function modeling dAl concentration C_{model} in surface water along the transect from station 7 (31°W, $x = 0$ m) to station 1 (58°W, $x = 2.82$ E6 m):

$$C_{model}(x) = \frac{a\,D_{Al}S_{Al}}{2hu}x^2 + \frac{b\,D_{Al}S_{Al}}{hu}x + c \quad (7)$$

where c is the dAl concentration at $x = 0$ m, that is, at station 7.

C_{model} with the parameters set above is shown in Figure 7 (red line) and is compared with the measured GApr08 dAl data. At each station, the average dAl bottle value was calculated by integration over the upper 100 m (C_{bottle}). Towed fish surface data (C_{fish}) are also shown for comparison with the modeled dAl distribution. As shown in Figure 7a, the model re-constructed the measured dAl distribution between the stations 7 and 2 reasonably well. Between the stations 2 and 1, the modeled concentrations are lower than both the bottle and towed fish data. The following discussion will address the model/data comparison, first between the stations 7 and 2 and then between the stations 2 and 1.

Despite a good fit between the modeled and measured dAl distribution between the stations 7 and 2, the absence of dAl removal associated with particle settling is inconsistent with our knowledge of the Al cycle, dAl being known to be removed from the water column by particle scavenging (Hydes, 1979; Orians & Bruland, 1986; Stoffyn & Mackenzie, 1982). Before discussing this scavenging flux, we first discuss the robustness of the different parameters in the present simplified model.

4.1.2. Assumptions and Limitation of the Model

Several assumptions were made for the dAl distribution model. Here we describe these and discuss how they could affect our results.

We assumed that the concentration of dAl was in a steady state (refer to Equation 6). This assumption was made because there was no dAl concentration time series data along 22°N. This type of assumption is very common in the context of projects based on a single cruise. There is excellent agreement in dAl concentrations over the upper 100 m between the three inter-comparison stations discussed above (GA02 2010, GA03 2011, and A16N 2013, refer to Figure 4) and the GApr08, which supports the assumption of a steady state in this layer in the subtropical North Atlantic.

NEC velocity was estimated from the global reanalysis GLORYS12V1 (1/12° horizontal resolution, 50 vertical levels), a product of the CMEMS that provides current velocities based on altimeter and other observed satellite data (temperature, salinity, etc.). The NEC velocity is highly dependent on the season with higher values in boreal summer (July/August) than in spring and fall (Arnault, 1987). This seasonality was visible within the GLORYS12V1 extracted NEC velocity values with higher velocity during the time of the cruise (June–August 2017, ~6 cm s^{-1}), compared with a 1-, 2-, or 3-year mean (~3 cm s^{-1}). To estimate the time the

water took to travel from the GApr08 station 7 to station 1, we used results from Lagrangian particle tracking experiments carried out in a previous study along the GApr08 (Artigue et al., 2020). These experiments tracked the origin of the water sampled during the GApr08 backward in time and indicated a transit time of ~2 years from the stations 7 to 1 at a 100 m depth. Therefore, it seems more realistic to extract a 2-year NEC velocity rather than a value for the time period of the cruise (June–August 2017). Moreover, this choice removed any seasonality in the current velocity estimate. The extracted mean NEC velocity over the upper 100 m, over the latitude range 21°–24°N, and over a 2-year period was 3.0 cm/s. However, given the distance between the stations 7 and 1 (2.82 E6 m), this results in a transit time of 3 years. Over a 3-year period, the mean NEC velocity was 2.8 cm/s. The difference in the average NEC velocity value over a 2-, or a 3-year period is not significant; for consistency, we chose a NEC velocity of 2.8 cm/s obtained over a 3-year period (August 16, 2014–August 16, 2017). Figure 7a presents how the NEC velocity impacts C_{model}. By applying the NEC velocity estimated for the period of our cruise (July 2017, blue solid line in Figure 7a), we find much lower dAl concentrations along the GApr08 compared with the C_{model} applying a 3-year mean NEC velocity (red line in Figure 7a). This supports our NEC velocity choice.

Similar to the NEC velocity, we chose an average dust deposition flux over a 3-year period (July 1, 2014–June 30, 2017) as this was the estimated time for the water to travel from station 7 to station 1. Dust transport and deposition is also seasonally dependent (Prospero et al., 2014). In summer, dust transport occurs at higher altitudes leading to relatively low dust deposition in the eastern tropical Atlantic, but maximum dust deposition in the western tropical Atlantic (Jickells et al., 2016; Kunde et al., 2019; Powell et al., 2015; Prospero et al., 2014). The MERRA-2 model also showed a higher dust deposition flux to surface waters of the western Atlantic compared with the east for July 2017 (Figure S2), while over 3 years, the trend is reversed (Figure 6). Figure 7a presents how the dust deposition impacts C_{model}. While applying the July 2017 dust flux to C_{model} (blue dashed line), we find lower dAl concentrations along the GApr08 compared with C_{model} using a 3-year mean dust flux (red line). This supports our choice of a 3-year mean dust flux for our model.

In the model, the Al content in dust was assumed to be that of the upper continental crust (Al = 8.2 ± 0.8% by mass, Rudnick & Gao, 2014). This is a common assumption (Han et al., 2008; Measures & Vink, 2000). The uncertainty of this estimate (±0.8%) results in negligible variations in C_{model} (Figure 7b, black solid and dotted lines).

Another assumption in the model was the solubility of Al from aerosols, which can vary depending on the nature of the deposition (wet or dry) or on the source region (Saharan dust, North American dust, etc.), which will further depend upon the season of collection (Baker et al., 2006, 2013; Shelley et al., 2018). In the above simulations, we used the Al solubility value of 6.8% from Baker et al. (2013) who report Al solubility variability across several oceanographic regions in the Atlantic. Their calculations account for both wet and dry deposition from ten large-scale research cruises and include the contribution from different aerosol sources over two three-month periods. This led to an estimated range of Al solubility from 6.1% to 18% for the Atlantic with a median value of 8.0%, and a value of ~6.8% for the eastern and subtropical North Atlantic regions, including most of the GApr08 section. Figure 7b presents how the variability in aerosol Al solubility could impact C_{model} (green solid and dashed lines).

From the above discussion, it appears that the largest uncertainty results from the Al solubility in dust. This will be extensively discussed in the following section.

4.1.3. Al Removal by Scavenging

The simple mass conservation equation defined in Equation 1 considered only advection and dust deposition. Here, we include a third term: the removal of dAl by scavenging. At the steady state, mass conservation implies that the removal of dAl from scavenging and advection must balance the input from dust deposition. Therefore, we estimated the dAl scavenging flux as the difference between dAl input from dust and advection, and dAl removal by advection. Given the uncertainties on the processes involved at station 1 (see Section 4.1.4), the mass balance calculation was performed on a single large box extending from the stations 7 to 2. The dAl scavenging flux was calculated as an average value (hereafter, F_{scav_avg}) over the length of the box, which leads to the following equation:

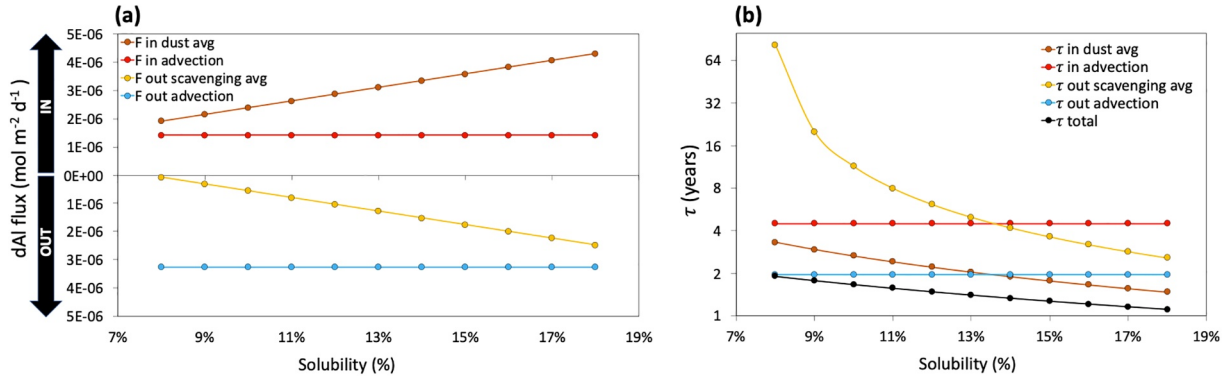

Figure 8. Dissolved Al fluxes (a) and partial residence times (b) obtained with solubilities varying from 8% to 18% in Equation 9. Note the log10 *y*-axis scale in (b).

$$F_{\text{scav\_avg}} = \left(C\left(\text{station 7}\right) - C\left(\text{station 2}\right)\right).\frac{uh}{\Delta x} + D_{\text{Al}} S_{\text{Al}}\, F_{\text{dust\_avg}} \tag{8}$$

where Δx = 2.37 E6 (distance between station 7 and 2), h = 100 m, C(station 7) = 1.39 E−5 mol m^{-3}, and C(station 2) = 3.19 E−5 mol m^{-3}. With an average dust flux value ($F_{\text{dust\_avg}}$) between the stations 7 and 2 (8 E−3 g m^{-2} d^{-1}), and unchanged D_{Al} and u values (3.02 mol kg^{-1} and 2.8 cm/s), this leads to the following equation:

$$\underbrace{F_{\text{scav\_avg}}}_{F_{\text{out scavenging avg}}} = \underbrace{1.42 \times 10^{-6}}_{F_{\text{in advection}}} - \underbrace{3.25 \times 10^{-6}}_{F_{\text{out advection}}} + \underbrace{S_{\text{Al}}\, 6.46 \times 10^{-4}}_{F_{\text{in dust avg}}} \tag{9}$$

Be aware that Equation 9 does not imply a mechanistic link between scavenging flux and solubility. It is a simple expression of a mass balance that states that removal of dAl from scavenging must equal the net inputs from advection and dust deposition over the box.

As stated above (Section 4.1.2), Equation 9 parameters u, D_{Al}, and $F_{\text{dust\_avg}}$ are well constrained, but Al solubility is more uncertain. The following discussion concentrates on the influence of aerosol dAl solubility on the mass balance.

If advection perfectly balances dust fluxes, that is, $F_{\text{scav\_avg}} = 0$, this requires a dAl solubility of ~7.7%. A lower solubility would imply a negative $F_{\text{scav\_avg}}$ value, which is impossible. In other words, our model suggests that S is ≥7.7%. Baker et al. (2013) report Al solubility from 6.1% to 18% for the Atlantic, with a median value of 8%. Our results are in excellent agreement with Baker et al. (2013).

Figure 8a displays the dAl input output fluxes for the GApr08 obtained with solubility ranging between 8% and 18%. With the median solubility of 8%, $F_{\text{scav\_avg}}$ is 7.7 E−8 mol m^{-2} d^{-1} , which is only 4% of the 1.9 E−6 mol m^{-2} d^{-1} dust flux; the remaining 96% dAl was removed from the box by advection. This illustrates the major role advection plays incontrolling dAl concentrations in the upper 100 m of the subtropical North Atlantic, compared to scavenging.

Processes that control the Al cycle are often discussed in terms of their residence times (τ). Residence time is defined, assuming a steady state, as follows:

$$\tau = \frac{Q}{\sum F_{\text{in}}} = \frac{Q}{\sum F_{\text{out}}} \tag{10}$$

where Q, F_{in}, and F_{out}, are the content and the fluxes in and out of a given reservoir, respectively.

This leads, here, to the following equation:

$$\tau_{\text{total}} = \frac{Q_{\text{Al}}}{F_{\text{in dust avg}} + F_{\text{in advection}}} = \frac{Q_{\text{Al}}}{F_{\text{out scavenging avg}} + F_{\text{out advection}}} \quad (11)$$

Here Q_{Al} is expressed as the dAl concentration mean in our box in mol m^{-2}, while the fluxes are in units of mol m^{-2} d^{-1}.

As there are several sources and sinks in our box model, we can also define partial residence time relative to each source and sink. Figure 8b displays the partial residence time (e.g., τ in dust avg, τ out scavenging avg) and the total residence time (τ_{total}) obtained with aerosol Al solubility ranging from 8% to 18%. It shows that the total residence time ranged between 2 and 1 years for S between 8% and 18%, respectively. This is consistent with previous estimates of dAl residence time between 1 and 8 years for the ~22°N in the Atlantic while including dust, advection, and mixing as dAl inputs (Han et al., 2008). The partial residence times for advection input (4.5 years) and output (2 years) stay constant irrespective of solubility. However, the partial residence times for dust input (3.3–1.5 years), and particularly for scavenging (82.4–2.6 years), vary with solubility (8%–18%). The partial residence time variation is larger for scavenging since the scavenging flux at a solubility of 8% is close to zero (Figure 8a). Again, these results highlight the major control advection has on the dAl distribution when compared to scavenging.

Overall, these results suggest that advection and dust deposition are the two main processes driving the increase in dAl from the stations 7 to 2, scavenging playing a secondary role. For a median and realistic Al solubility of 8%, dAl removal by scavenging is insignificant in this study area. In the unlikely case of an extreme 18% solubility, the scavenging flux should be included in the model (Figure 8).

We recognize that assuming a constant scavenging rate across the transect is a crude approximation. Scavenging fluxes are usually parameterized as a function of dissolved trace metal concentrations and/or particle concentrations and/or export (e.g., van Hulten et al., 2013), and therefore, are likely to be variable across the transect. However, this simplified approach allows an estimation of its order of magnitude and therefore, of its importance relative to the other processes involved in the Al cycle in this area.

4.1.4. Origin of the dAl Enrichment in the Western Subtropical North Atlantic

For a realistic North Atlantic solubility range, the model reproduces the progressive dAl concentration increase from the stations 7 to 2, but did not capture the steep increase in dAl concentration between the stations 2 and 1. For C_{model} with a solubility of 8% (Figure 7b, green dashed line), there was up to a ~4 nmol/kg difference between the modeled and measured dAl values. Considering that these dAl observations are representative of a 3° meridional band between 21°N and 24°N (Δy = 3.33 E5 m distance), where dust deposition and the NEC are relatively homogeneous, this offset corresponds to an additional flux of 3 E5 mol/d at station 1 calculated as follows:

$$F_{\text{additional source}} = \left(C_{\text{bottle}}\left(\text{stn.1}\right).u - C_{\text{model}-\text{scav}}\left(\text{stn.1}\right).u\right)\left(\Delta y\,.\,h\right) \quad (12)$$

This missing input flux implies a source of dAl that is either not included or not correctly parametrized in our model. In the following discussion, we will refer to this difference of 3 E5 mol/day as the "additional source" of dAl needed to explain the dAl distribution in the western subtropical North Atlantic along the GApr08.

The MERRA-2 includes most species of aerosol from both natural and anthropogenic sources (dust, sea salt, black carbon, organic carbon, and sulfate, Gelaro et al., 2017). The increase in dAl between the stations 2 and 1 could reflect the impact of another aerosol type, not included in the MERRA-2, with a higher solubility and/or with an Al concentration in an excess of typical crustal material. With increased aerosol Al solubility and/or concentration, the modeled concentrations along the GApr08 would gradually increase between the stations 2 and 1, as the westward advection term should provide a continuous increase in the model, which does not correspond to the observations, that is, a sharp increase in dAl concentration west of station 2. This dAl increase rather suggests a disturbance in the westward advection flux, most probably current branches joining the NEC from the west or the south, as shown in Figure S3.

A tongue of lower salinity surface water was observed at the western edge of the GApr08 section (salinity <35 for the westernmost towed fish samples and salinity <37 shallower than 27 m at the stations 1 and 2, Figure S4). Surface salinity maps allowed us to attribute this low salinity to the Amazon River plume (Artigue et al., 2020). With a dAl concentration of 3 E–4 mol/m^3 and a mean flow rate estimated at 2 E10 m^3/day (Gaillardet et al., 2003), the Amazon River delivers approximately 5 E6 mol/day of dAl to the Atlantic. In order to explain the additional source of dAl to the upper 100 m of the western subtropical North Atlantic (Figure 7), 5% of this flux would have to pass through estuaries and reach the western part of the GApr08 transect some 2,500 km away. This seems unrealistic as much of the riverine dAl inputs is known to be quickly scavenged in estuaries and is considered to not represent a significant source of dAl to the open ocean (Brown et al., 2010; Hydes & Liss, 1977; Mackin & Aller, 1984; Orians & Bruland, 1986). Moreover, no increase in dAl concentration was recorded within the Amazon River plume during the GA02 (Middag, van Hulten, et al., 2015), during the same time of the year as the GApr08, contrary to observations of elevated dissolved iron (Rijkenberg et al., 2014), and contrary to elevated dissolved iron and dissolved 232 thorium ~1,900 km from the river's mouth (AE1410, Hayes et al., 2017). Therefore, it seems unrealistic that the Amazon River explains the dAl enrichment in the west of our section.

The Amazon suspended sediment discharge is estimated at 8 E8 tons/year (Martinez et al., 2009). Assuming a concentration of Al in the upper continental crust of 0.003 mol/g (Rudnick & Gao, 2014), the Amazon river delivers 7 E9 mol/day of pAl to the western North Atlantic. The dissolution of terrigenous particle material delivered by rivers to the ocean can have a large impact on the global cycling of some elements (Jeandel & Oelkers, 2015; Radic et al., 2011). Much of these particles settle onto continental margins, but for several elements, a small but nonzero fraction dissolves and can be transported over long distances, for instance 3%–5% for neodymium (Arsouze et al., 2009; Jeandel et al., 2011; Lacan & Jeandel, 2005). pAl dissolution in the range of 1%–5% has been assumed by Brown and Bruland (2009) to estimate the dAl flux delivered by the Columbia River to coastal waters. In this study, the dissolution and transport of only ~0.004% of the 7 E9 mol/day pAl delivered to the continental margin by the Amazon River would be sufficient to explain the dAl enrichment in the west of our section.

The Lesser Antilles, a group of mostly volcanic islands in the Caribbean Sea, are also a potential source of dAl that is close to the western part of the GApr08 cruise (less than 400 km between Guadeloupe and the GApr08 surface transect, Figure 1). Velocity fields over the upper 100 m indeed suggest that waters impacted by the Lesser Antilles may reach the western end of the GApr08 (Figure S3). This led us to investigate erosion and chemical weathering in the Lesser Antilles as possible sources of dAl to our section, particularly as the rates for these processes are high due to the Lesser Antilles' easily weathered volcanic material, pronounced relief, and high runoff rates (Gaillardet et al., 2011; Rad et al., 2013).

The mechanical erosion rate for Guadeloupe is estimated between 800 and 4,000 t/km^2/year (Rad et al., 2006). Assuming an Al concentration in the Guadeloupe bulk regolith of 0.006 mol/g (i.e., 15.25% by weight, mean value, Buss et al., 2010), the Lesser Antilles could deliver between 6 E7 and 3 E8 mol/day of pAl to the surrounding oceans. The dissolution and transport of only 0.1%–0.5% of this pAl could explain the dAl enrichment observed west of our section.

Due to the very low content of organic matter in the rivers of the lesser Antilles, uncomplexed dAl is considered to be rapidly removed from the solution by particle scavenging (Mackin & Aller, 1984). Moreover, the ratio of pAl fluxes delivered by rivers to the corresponding dAl being estimated at 1,000, a direct dAl flux from the lesser Antilles would be lower than the 3 E5 mol/day needed to explain the additional source (Gaillardet et al., 2003; Jeandel & Oelkers, 2015; Viers et al., 2009). Therefore, it seems unrealistic that a direct dAl source from the Lesser Antilles (which does not include the dAl from the dissolution of pAl from the river) could explain the dAl enrichment in the west of our section.

In addition, Lambelet et al. (2016) measured a shift toward higher neodymium concentrations and radiogenic neodymium isotopic compositions along the GA02 between 19° and 25°N, compared to northern stations. They suggested this isotopic signature reflected lithogenic inputs from the Lesser Antilles rather than from the Amazon or Orinoco rivers, or from volcanic ash.

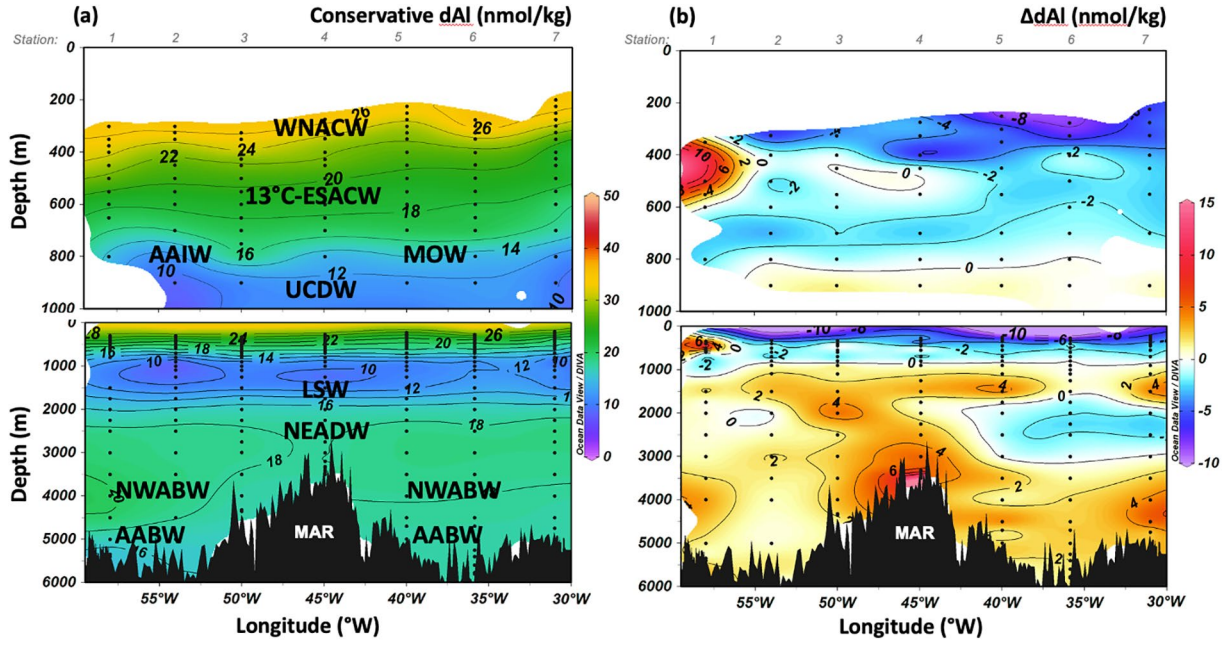

Figure 9. (a) GApr08 "conservative" dissolved aluminum (dAl) section indicating the dominant water masses found along GApr08: West North Atlantic Central Water (WNACW), Antarctic Intermediate Water (AAIW), Upper Circumpolar Deep Water (UCDW), Labrador Sea Water (LSW), North East Atlantic Deep Water (NEADW), North West Atlantic Bottom Water (NWABW), Antarctic Bottom Water (AABW). For the exact distribution of these water masses, see Artigue et al. (2020). (b) GApr08 "biogeochemical" ΔdAl section. Data points are represented by black dots, top panels are a zoom in the upper 1,000 m.

Overall, this suggests that dissolution of continental pAl eroded form the Lesser Antilles, or less likely, delivered by the Amazon River, could explain our observations of elevated dAl in surface waters of the western subtropical Atlantic. As described below, a dAl enrichment found along the western edge of the GApr08 between 400 and 500 m reinforces this conclusion.

4.2. Intermediate and Deep dAl Distributions

Along most of the section, dAl concentrations decrease from the surface to a minimum (10–15 nmol/kg) at depths between 700 and 1,500 m (Figures 2a and 2b). Concentrations then increase to ~20 nM by 4,000 m, and stabilize around this value down to the seafloor. Two local features differ from this homogeneity, (a) a clear enrichment above the Snakepit hydrothermal site (station 4, at the MAR), and (b) an enrichment at ~400 m at the westernmost station 1.

To investigate if the dAl distribution was driven by water mass transport and/or biogeochemical processes, we used the results of the eOMPA specifically carried out for this cruise, for data deeper than ~200–300 m (Artigue et al., 2020). This eOMPA identified the mixing fractions of the major water masses along the GApr08. These water masses were defined at specific locations and called end-members. All the end-members of this eOMPA were defined from the GEOTRACES section cruises where dAl concentrations were available. End-member locations and dAl concentrations are shown in Figure 1 and Table S1, respectively. This allowed us to calculate a dAl "conservative" GApr08 section, that is, where the dAl distribution results from water mass transport and physical mixing (Figure 9a).

The dominant water masses found along the GApr08 are indicated in Figure 9a. The "conservative" dAl section reflected the main features of the measured dAl section (Figure 2a). Notably, between 100 and 500 m, the high surface dAl carried by the West North Atlantic Central Water (WNACW). Between 800 and 1,750 m, the low dAl tongue carried by Antarctic Intermediate Water, Upper Circumpolar Deep Water and Labrador Sea Water. Between 2,000 and 4,000 m, the higher dAl concentrations carried by North East Atlantic Deep Water and North West Atlantic Bottom Water. Finally, at bottom depths, the lower dAl concentrations carried by Antarctic Bottom Water. These conservative dAl properties, transported within water

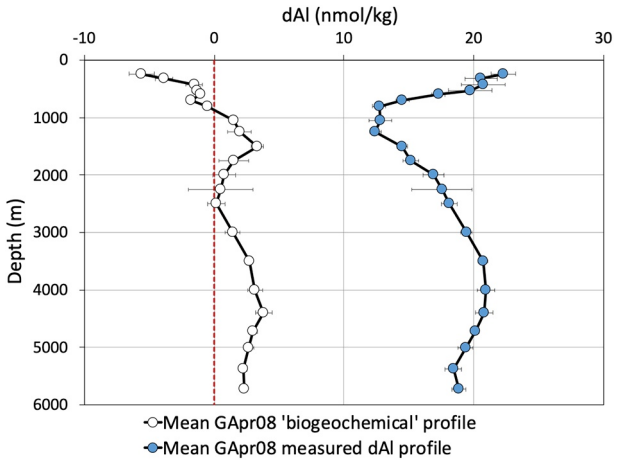

Figure 10. Mean "biogeochemical" ΔdAl profile (white dots) and mean measured dissolved aluminum (dAl) profiles (blue dots) of the seven stations of GApr08 with their respective standard errors. Note that the two local dAl inputs were removed from the analysis (i.e., 400–500 m at station 1, and deeper than 2,500 m at station 4). The profiles were calculated by including samples over a 100 m range for samples between 200 and 1,100 m depth, and over 200 m range between 4,000 and 5,000 m.

masses, seem to dominate the dAl distribution (Figures 2a and 9a) with the exception of some local features.

The subtraction of the GApr08 measured dAl section data (Figure 2a) from the "conservative" section (Figure 9a) allowed us to calculate a residual "biogeochemical" ΔdAl section (Figure 9b). This biogeochemical ΔdAl section, represents the part of the dAl signal that does not result from water mass transport and therefore, results from biogeochemical processes occurring between the end-member locations and the measured GApr08 section (Figure 1). These biogeochemical processes include dissolved-particulate exchange and sedimentary or hydrothermal inputs. Positive and negative ΔdAl values reveal dAl input and removal, respectively, due to biogeochemical processes.

Two local features are clearly visible in the biogeochemical ΔdAl section at the stations 1 and 4 (Figure 9b).

At station 1, a ΔdAl maximum between 400 and 500 m implies that 10 nmol/kg of dAl was added to the dAl transported by water masses (contribution of ~66% WNACW, ~20% 13°C-ESACW, and ~13% MW, Artigue et al., 2020). As suggested for surface waters, this subsurface ΔdAl enrichment could reflect the dissolution of erosion products delivered from nearby margins (e.g., Lesser Antilles and/or less likely the Amazon River).

Station 4 targeted the Snakepit hydrothermal site (23,367°N, 44,95°W, 3,500 m depth, Beaulieu & Szafranski, 2019, and references therein). Deeper than 3,300 m, a positive anomaly in the beam attenuation profile was observed at this station (Figure S5), indicative of an increased suspended particle content associated with the neutrally buoyant hydrothermal plume. Deeper than 3,340 m, that is, ~170 m above the sea floor, ΔdAl reached values between 8 and 16 nmol/kg (Figure 9b), enriching dAl to a maximum of 32.5 nmol/kg at 3,500 m (Figure 2a). This would suggest that up to 50% of the measured dAl concentration at Snakepit can be attributed to the hydrothermal vent. Note that a dissolved iron concentration maximum at 3,300 m at station 4 has also been attributed to hydrothermal venting (Kunde et al., 2019). Hydrothermally derived dAl has been previously reported for the MAR (up to 53 nmol/kg at the TAG vent site, Lunel et al., 1990; Measures et al., 2015). In the Southeast Pacific Rise, hydrothermalism may explain dAl plumes extending over several thousand kilometers (Lupton et al., 1993; Resing et al., 2015). Note that we did not observe any lateral transport of high dAl concentration at the GApr08 stations 3 and 5 (located ~500 km away from the MAR).

Except from the two specific features discussed above, the rest of the ΔdAl section is mostly zonally homogeneous. Figure 10 shows the ΔdAl profile calculated as a zonal mean of the 7 stations (excluding the 2 local features discussed above).

Negative ΔdAl values between 225 and 800 m (from −6 nmol/kg to 0 nmol/kg) revealed a clear and significant removal of dAl in this layer. The calculated ΔdAl values were well above uncertainties associated to our data and the prescribed end-member dAl concentrations (~0.3 nmol/kg for both). This result is particularly surprising, because this layer is associated with high dAl values (>20 nmol/kg), and is usually interpreted as reflecting the effect of local dust dissolution (Gehlen et al., 2003; Han et al., 2008; Maring & Duce, 1987; Measures et al., 2010; van Hulten et al., 2013). However, we argue that the high values reflect the advection of remotely enriched waters, with significant removal along their flow path. This 225–800 m layer is composed mainly of WNACW and a small fraction of 13°C-ESACW that, within the eOMPA, have their end-members located in the Sargasso Sea and Cape Basin, respectively (Figure 1). We therefore argue that between these locations and the GApr08 section, the net effect of biogeochemical processes was to remove dAl, rather than to add dAl as usually assumed. Most studies attribute dAl removal to, (a) passive adsorption onto particle surfaces followed by sinking (Bruland & Lohan, 2006; Orians & Bruland, 1986) or, (b) active diatom uptake (Al is incorporated during opal formation as a replacement of silicium, Gehlen

et al., 2002; Mackenzie et al., 1978; Stoffyn, 1979). Between 225 and 800 m, diatom opal formation is not expected (below the euphotic zone). Therefore, scavenging onto particles, notably mineral dust particles (following partial dissolution of dust in surface waters, described in Section 4.1.3 in the upper 100 m), seems a more likely cause. Scavenging of dAl was further supported by the fact that the negative ΔdAl values were well correlated with particle abundances as indicated by the beam attenuation profiles (Figure S5). This is not the first time that dust has been postulated to act as a sink rather than a source of an element. This was observed for dissolved iron during a mesocosm experiment in the Mediterranean Sea where the addition of dust lead to a decrease of dissolved iron concentration attributed to scavenging (Wagener et al., 2010; Wuttig et al., 2013; Ye et al., 2011).

Below 800 m, ΔdAl was positive with consistent values of ∼2.5 nmol/kg down to the seafloor, except between 1,750 and 3,000 m where ΔdAl nears zero. This latter feature was the result of negative values in the east (−2.5) and positive values in the west (+2.5), which cancel out (Figure 9b). In fact, if the seven data points (out of 81 points below 800 m) with negatives ΔdAl were not included in our calculation of the mean ΔdAl profile, we would observe a homogeneous ΔdAl profile at ∼2.5 nmol/kg between 800 m and the seafloor. Overall, these data reveal that over this depth range, the dAl distribution is mostly dominated by addition. Internal sources of dAl due to desorption from particles (reversible scavenging) has been suggested in recent studies (Middag, van Hulten, et al., 2015; van Hulten et al., 2013). This process, initially proposed for thorium (Bacon & Anderson, 1982; Nozaki et al., 1981), has also been proposed as a significant process, notably at depth, in the internal cycles of rare earth elements (Nozaki & Alibo, 2003), copper (Little et al., 2013), iron (Abadie et al., 2017), and zinc (Weber et al., 2018).

Sediment resuspension processes can also act as a source of dAl at depth (Middag et al., 2009, 2012; Middag, van Hulten, et al., 2015; Moran & Moore, 1991; van Hulten et al., 2013). The beam attenuation profiles measured during the GApr08 (Figure S5) show particle increases from about 4,000 m down to the seafloor, consistent with sediment resuspensions. The ΔdAl results do suggest a dAl source at those depths. However, this source is not larger below 4,000 m than elsewhere in the water column below 1,000 m. Therefore, our results do not point to any specific dAl source associated to particle resuspension above the bottom.

5. Conclusions

Surface dAl concentrations, measured along the GApr08 section in the subtropical North Atlantic, displayed a marked westwards increasing gradient. Using a mass balance model that included advection, dust deposition, and scavenging terms, we showed that this increase was not just due to dust deposition, but that advection is essential in driving this gradient in the subtropical North Atlantic and therefore, needs to be incorporated into future dAl studies. In this surface layer (100 m), scavenging of dAl onto particles appears to play a much smaller role than advection in driving dAl distribution.

In the westernmost part of the GApr08 section surface layer, an additional dAl flux of ∼3 E5 mol/day was required to explain the dAl concentrations. We suggest that the most likely source is the dissolution of eroded continental particles delivered to the margins from the Lesser Antilles and/or, less likely, the Amazon River.

By utilizing the results from an eOMPA for the GApr08 cruise (Artigue et al., 2020), we estimated and separated the "biogeochemical" from the "conservative" component of the dAl section. The conservative component dominated the dAl distribution. However, it was insufficient to explain all the features that were observed. The biogeochemical ΔdAl section highlighted two local features: a dAl enrichment between 400 and 500 m at the westernmost station and a hydrothermal enrichment from the Snakepit hydrothermal site that doubled the local dAl concentrations. Except from these two features, the ΔdAl section is mostly zonally homogeneous. Despite high dust deposition fluxes in the subtropical North Atlantic, the ΔdAl profile suggests that, between 200 and 800 m, removal by scavenging exceeds inputs from dust deposition and dissolution at the basin scale. From 800 m to the seafloor, the ΔdAl profile showed an addition of dAl, likely due to reversible scavenging. Just above the bottom, this profile does not provide evidence for dAl addition linked to sediment resuspension.

Overall, this study highlights the importance of quantitatively considering water mass transport processes to interpret dAl distributions throughout the water column at the local to basin scale. First, in regions of significant horizontal gradients and significant flows (particularly in the surface layers), the process of advection is significant and should not be neglected. Second, by removing the portion of the dAl signal due to water mass transport, we have gained new insights into the Al biogeochemical cycle of the subtropical North Atlantic.

Data Availability Statement

The data of this study are publicly available from the British Oceanographic Data Centre under doi:10/f9gg. The data have also been submitted to the GEOTRACES Intermediate Data Product 2021.

Acknowledgments
The authors thank K. Kunde and D. G. Santana for sampling alongside the Captain and crew of the RRS James Cook during GApr08. The authors thank J. Gaillardet for his help about the Lesser Antilles erosion and weathering. The authors thank J. K. Klar for the GA06 dAl data and for the helpful scientific discussion. The authors thank A. Carret for the help with MATLAB. The authors thank J. D. Milliman, R. Middag, and K. Kunde for the helpful scientific discussion. The authors thank the reviewers of this study, one anonymous, and J. Resing for constructive comments that helped improve the manuscript. The French Ministry of Higher Education, Research and Innovation (MESRI) funded through the University Toulouse III the Ph.D. fellowship of L. Artigue. The French National Centre for Scientific Research (CNRS) funded F. Lacan. NERC funded C. Mahaffey (NE/N001979/1) and M.C. Lohan (NE/N001125/1).

References

Abadie, C., Lacan, F., Radic, A., Pradoux, C., & Poitrasson, F. (2017). Iron isotopes reveal distinct dissolved iron sources and pathways in the intermediate versus deep Southern Ocean. *Proceedings of the National Academy of Sciences of the United States of America*, *114*(5), 858–863. https://doi.org/10.1073/pnas.1603107114

Arnault, S. (1987). Tropical Atlantic geostrophic currents and ship drifts. *Journal of Geophysical Research*, *92*, 5076–5088.

Arsouze, T., Dutay, J.-C., Lacan, F., & Jeandel, C. (2009). Reconstructing the Nd oceanic cycle using a coupled dynamical-biogeochemical model. *Biogeosciences*, *6*(12), 2829–2846. https://doi.org/10.5194/bg-6-2829-2009

Artigue, L., Lacan, F., van Gennip, S., Lohan, M. C., Wyatt, N. J., Woodward, E. M. S., et al. (2020). Water mass analysis along 22°N in the subtropical North Atlantic for the JC150 cruise (GEOTRACES, GApr08). *Deep Sea Research Part I: Oceanographic Research Papers*, *158*, 103230. https://doi.org/10.1016/j.dsr.2020.103230

Bacon, M. P., & Anderson, R. F. (1982). Distribution of thorium isotopes between dissolved and particulate forms in the deep sea. *Journal of Geophysical Research*, *87*(C3), 2045–2056. https://doi.org/10.1029/JC087iC03p02045

Baker, A. R., Adams, C., Bell, T. G., Jickells, T. D., & Ganzeveld, L. (2013). Estimation of atmospheric nutrient inputs to the Atlantic Ocean from 50°N to 50°S based on large-scale field sampling: Iron and other dust-associated elements. *Global Biogeochemical Cycles*, *27*(3), 755–767. https://doi.org/10.1002/gbc.20062

Baker, A. R., Jickells, T. D., Witt, M., & Linge, K. L. (2006). Trends in the solubility of iron, aluminium, manganese and phosphorus in aerosol collected over the Atlantic Ocean. *Marine Chemistry*, *98*(1), 43–58. https://doi.org/10.1016/j.marchem.2005.06.004

Barrett, P. M., Resing, J. A., Buck, N. J., Landing, W. M., Morton, P. L., & Shelley, R. U. (2015). Changes in the distribution of Al and particulate Fe along A16N in the eastern North Atlantic Ocean between 2003 and 2013: Implications for changes in dust deposition. *Marine Chemistry*, *177*, 57–68. https://doi.org/10.1016/j.marchem.2015.02.009

Beaulieu, S. E., & Szafranski, K. (2019). *InterRidge global database of active submarine hydrothermal vent fields version 3.4*. Retrieved from https://vents-data.interridge.org/ventfields

Brown, M. T., & Bruland, K. W. (2008). An improved flow-injection analysis method for the determination of dissolved aluminum in seawater. *Limnology and Oceanography: Methods*, *6*(1), 87–95. https://doi.org/10.4319/lom.2008.6.87

Brown, M. T., & Bruland, K. W. (2009). Dissolved and particulate aluminum in the Columbia River and coastal waters of Oregon and Washington: Behavior in near-field and far-field plumes. *Estuarine, Coastal and Shelf Science*, *84*(2), 171–185. https://doi.org/10.1016/j.ecss.2009.05.031

Brown, M. T., Lippiatt, S. M., & Bruland, K. W. (2010). Dissolved aluminum, particulate aluminum, and silicic acid in northern Gulf of Alaska coastal waters: Glacial/riverine inputs and extreme reactivity. *Marine Chemistry*, *122*(1), 160–175. https://doi.org/10.1016/j.marchem.2010.04.002

Bruland, K. W., & Lohan, M. C. (2006). 6.02 controls of trace metals in seawater (Vol. 25).

Buss, H. L., White, A. F., Dessert, C., Gaillardet, J., Blum, A. E., & Sak, P. B. (2010). Depth profiles in a tropical, volcanic critical zone observatory : Basse-Terre, Guadeloupe (Vol. 4).

de Boyer Montégut, C. (2004). Mixed layer depth over the global ocean: An examination of profile data and a profile-based climatology. *Journal of Geophysical Research*, *109*(C12), C12003. https://doi.org/10.1029/2004JC002378

Fieux, M. (2010). *L'océan planétaire* (p. 165). Les Presses de l'ENSTA.

Gaillardet, J., Rad, S., Rive, K., Louvat, P., Gorge, C., Allegre, C. J., & Lajeunesse, E. (2011). Orography-driven chemical denudation in the Lesser Antilles: Evidence for a new feed-back mechanism stabilizing atmospheric CO_2. *American Journal of Science*, *311*(10), 851–894. https://doi.org/10.2475/10.2011.02

Gaillardet, J., Viers, J., Dupré, B., & Drever, J. I. (2003). Trace elements in river waters. In H. D. Holland, & K. K. Turekian (Eds.), Surface and ground water, weathering, and soils (Treatise on Geochemistry, Vol. 5, pp. 225–272). Elsevier-Pergamon. https://doi.org/10.1016/b0-08-043751-6/05165-3

Gehlen, M., Beck, L., Calas, G., Flank, A.-M., Van Bennekom, A. J., & Van Beusekom, J. E. E. (2002). Unraveling the atomic structure of biogenic silica: Evidence of the structural association of Al and Si in diatom frustules. *Geochimica et Cosmochimica Acta*, *66*(9), 1601–1609. https://doi.org/10.1016/S0016-7037(01)00877-8

Gehlen, M., Heinze, C., Maier-Reimer, E., & Measures, C. I. (2003). Coupled Al-Si geochemistry in an ocean general circulation model: A tool for the validation of oceanic dust deposition fields? *Global Biogeochemical Cycles*, *17*(1). https://doi.org/10.1029/2001GB001549

Gelaro, R., McCarty, W., Suárez, M. J., Todling, R., Molod, A., Takacs, L., et al. (2017). The Modern-Era Retrospective Analysis for Research and Applications, Version 2 (MERRA-2). *Journal of Climate*, *30*(14), 5419–5454. https://doi.org/10.1175/JCLI-D-16-0758.1

Global Modeling and Assimilation Office (GMAO). (2015). MERRA-2 tavgM_2d_adg_Nx : 2d, monthly mean, time-averaged, single-level, assimilation, aerosol diagnostics (extended) V5.12.4. Goddard Earth Sciences Data and Information Services Center (GES DISC). https://doi.org/10.5067/RZIK2TV7PP38

Han, Q., Moore, J. K., Zender, C., Measures, C., & Hydes, D. (2008). Constraining oceanic dust deposition using surface ocean dissolved Al. *Global Biogeochemical Cycles*, *22*(2). https://doi.org/10.1029/2007GB002975

Hayes, C. T., Rosen, J., McGee, D., & Boyle, E. A. (2017). Thorium distributions in high- and low-dust regions and the significance for iron supply. *Global Biogeochemical Cycles*. https://doi.org/10.1002/2016GB005511

Hydes, D. J. (1979). Aluminum in seawater: Control by inorganic processes. *Science*, *205*, 1260–1262. https://doi.org/10.1126/science.205.4412.1260

Hydes, D. J., de Lange, G. J., & de Baar, H. J. W. (1988). Dissolved aluminium in the Mediterranean. *Geochimica et Cosmochimica Acta*, *52*(8), 2107–2114. https://doi.org/10.1016/0016-7037(88)90190-1

Hydes, D. J., & Liss, P. S. (1977). The behaviour of dissolved aluminium in estuarine and coastal waters. *Estuarine and Coastal Marine Science*, *5*(6), 755–769. https://doi.org/10.1016/0302-3524(77)90047-0

Hydes, D. J., Statham, P. J., & Burton, J. D. (1986). A vertical profile of dissolved trace metals (Al, Cd, Cu, Mn, Ni) over the median valley of the mid Atlantic ridge, 43°N: Implications for Hydrothermal activity. *The Science of the Total Environment*, *49*, 133–145. https://doi.org/10.1016/0048-9697(86)90236-6

Jeandel, C., & Oelkers, E. H. (2015). The influence of terrigenous particulate material dissolution on ocean chemistry and global element cycles. *Chemical Geology*, *395*, 50–66. https://doi.org/10.1016/j.chemgeo.2014.12.001

Jeandel, C., Peucker Ehrenbrink, B., Jones, M. T., Pearce, C. R., Oelkers, E. H., Godderis, Y., et al. (2011). Ocean margins: The missing term in oceanic element budgets? *Eos, Transactions, American Geophysical Union*, *92*(26), 217–218. https://doi.org/10.1029/2011EO260001

Jickells, T. D., An, Z. S., Andersen, K. K., Baker, A. R., Bergametti, G., Brooks, N., et al. (2005). Global iron connections between desert dust, ocean biogeochemistry, and climate. *Science*, *308*(5718), 67–71. https://doi.org/10.1126/science.1105959

Jickells, T. D., Baker, A. R., & Chance, R. (2016). Atmospheric transport of trace elements and nutrients to the oceans. *Philosophical Transactions of the Royal Society A: Mathematical, Physical and Engineering Sciences*, *374*(2081), 20150286. https://doi.org/10.1098/rsta.2015.0286

Jickells, T. D., Church, T., Veron, A., & Arimoto, R. (1994). Atmospheric inputs of manganese and aluminium to the Sargasso Sea and their relation to surface water concentrations. *Marine Chemistry*, *46*(3), 283–292. https://doi.org/10.1016/0304-4203(94)90083-3

Kunde, K., Wyatt, N. J., González-Santana, D., Tagliabue, A., Mahaffey, C., & Lohan, M. C. (2019). Iron distribution in the subtropical North Atlantic: The pivotal role of colloidal iron. *Global Biogeochemical Cycles*, *33*, 1532, 1547. https://doi.org/10.1029/2019GB006326

Lacan, F., & Jeandel, C. (2005). Acquisition of the neodymium isotopic composition of the North Atlantic Deep Water. *Geochemistry, Geophysics, Geosystems*, *6*(12). https://doi.org/10.1029/2005GC000956

Lambelet, M., van de Flierdt, T., Crocket, K., Rehkämper, M., Kreissig, K., Coles, B., et al. (2016). Neodymium isotopic composition and concentration in the western North Atlantic Ocean: Results from the GEOTRACES GA02 section. *Geochimica et Cosmochimica Acta*, *177*, 1–29. https://doi.org/10.1016/j.gca.2015.12.019

Little, S. H., Vance, D., Siddall, M., & Gasson, E. (2013). A modeling assessment of the role of reversible scavenging in controlling oceanic dissolved Cu and Zn distributions. *Global Biogeochemical Cycles*, *27*(3), 780–791. https://doi.org/10.1002/gbc.20073

Lunel, T., Rudnicki, M., Elderfield, H., & Hydes, D. (1990). Aluminium as a depth-sensitive tracer of entrainment in submarine hydrothermal plumes. *Nature*, *344*(6262), 137–139. https://doi.org/10.1038/344137a0

Lupton, J. E., Baker, E. T., Mottl, M. J., Sansone, F. J., Wheat, C. G., Resing, J. A., et al. (1993). Chemical and physical diversity of hydrothermal plumes along the East Pacific Rise, 8°45′N to 11°50′N. *Geophysical Research Letters*, *20*(24), 2913–2916. https://doi.org/10.1029/93GL00906

Mackenzie, F. T., Stoffyn, M., & Wollast, R. (1978). Aluminum in seawater: Control by biological activity. *Science*, *199*(4329), 680–682. https://doi.org/10.1126/science.199.4329.680

Mackin, J. E., & Aller, R. C. (1984). Processes affecting the behavior of dissolved aluminum in estuarine waters. *Marine Chemistry*, *14*(3), 213–232. https://doi.org/10.1016/0304-4203(84)90043-4

Maring, H. B., & Duce, R. A. (1987). The impact of atmospheric aerosols on trace metal chemistry in open ocean surface seawater, 1. Aluminum. *Earth and Planetary Science Letters*, *84*(4), 381–392. https://doi.org/10.1016/0012-821X(87)90003-3

Martinez, J. M., Guyot, J. L., Filizola, N., & Sondag, F. (2009). Increase in suspended sediment discharge of the Amazon River assessed by monitoring network and satellite data. *Catena*, *79*(3), 257–264. https://doi.org/10.1016/j.catena.2009.05.011

Measures, C. I., & Brown, E. T. (1996). Estimating dust input to the Atlantic Ocean Using surface water aluminium concentrations. In S. Guerzoni, & R. Chester (Eds.), *The impact of desert dust across the mediterranean* (pp. 301–311). Springer Netherlands. https://doi.org/10.1007/978-94-017-3354-0_30

Measures, C. I., Brown, M. T., & Vink, S. (2005). Dust deposition to the surface waters of the western and central North Pacific inferred from surface water dissolved aluminum concentrations. *Geochemistry, Geophysics, Geosystems*, *6*(9). https://doi.org/10.1029/2005GC000922

Measures, C. I., Edmond, J. M., & Jickells, T. D. (1986). Aluminium in the northwest Atlantic. *Geochimica et Cosmochimica Acta*, *50*(7), 1423–1429. https://doi.org/10.1016/0016-7037(86)90315-7

Measures, C. I., Hatta, M., Fitzsimmons, J., & Morton, P. (2015). Dissolved Al in the zonal N Atlantic section of the US GEOTRACES 2010/2011 cruises and the importance of hydrothermal inputs. *Deep Sea Research Part II: Topical Studies in Oceanography*, *116*, 176–186. https://doi.org/10.1016/j.dsr2.2014.07.006

Measures, C. I., Sato, T., Vink, S., Howell, S., & Li, Y. H. (2010). The fractional solubility of aluminium from mineral aerosols collected in Hawaii and implications for atmospheric deposition of biogeochemically important trace elements. *Marine Chemistry*, *120*(1), 144–153. https://doi.org/10.1016/j.marchem.2009.01.014

Measures, C. I., & Vink, S. (2000). On the use of dissolved aluminum in surface waters to estimate dust deposition to the ocean. *Global Biogeochemical Cycles*, *14*(1), 317–327. https://doi.org/10.1029/1999GB001188

Menzel Barraqueta, J.-L., Klar, J. K., Gledhill, M., Schlosser, C., Shelley, R., Planquette, H., et al. (2018). Atmospheric aerosol deposition fluxes over the Atlantic Ocean: A GEOTRACES case study. *Biogeosciences Discussions*, 1–25. https://doi.org/10.5194/bg-2018-209

Menzel Barraqueta, J.-L., Schlosser, C., Planquette, H., Gourain, A., Cheize, M., Boutorh, J., et al. (2018). Aluminium in the North Atlantic Ocean and the Labrador Sea (GEOTRACES GA01 section): Roles of continental inputs and biogenic particle removal. *Biogeosciences Discussions*, 1–28. https://doi.org/10.5194/bg-2018-39

Middag, R., de Baar, H. J. W., Laan, P., & Bakker, K. (2009). Dissolved aluminium and the silicon cycle in the Arctic Ocean. *Marine Chemistry*, *115*(3), 176–195. https://doi.org/10.1016/j.marchem.2009.08.002

Middag, R., de Baar, H. J. W., Laan, P., & Huhn, O. (2012). The effects of continental margins and water mass circulation on the distribution of dissolved aluminum and manganese in Drake Passage. *Journal of Geophysical Research*, *117*. https://doi.org/10.1029/2011jc007434

Middag, R., Séférian, R., Conway, T. M., John, S. G., Bruland, K. W., & de Baar, H. J. W. (2015). Intercomparison of dissolved trace elements at the Bermuda Atlantic Time Series station. *Marine Chemistry*, *177*, 476–489. https://doi.org/10.1016/j.marchem.2015.06.014

Middag, R., van Hulten, M. M. P., Van Aken, H. M., Rijkenberg, M. J. A., Gerringa, L. J. A., Laan, P., & de Baar, H. J. W. (2015). Dissolved aluminium in the ocean conveyor of the West Atlantic Ocean: Effects of the biological cycle, scavenging, sediment resuspension and hydrography. *Marine Chemistry*, *177*, 69–86. https://doi.org/10.1016/j.marchem.2015.02.015

Moran, S. B., & Moore, R. M. (1991). The potential source of dissolved aluminum from resuspended sediments to the North Atlantic Deep Water. *Geochimica et Cosmochimica Acta*, *55*(10), 2745–2751. https://doi.org/10.1016/0016-7037(91)90441-7

Nozaki, Y., & Alibo, D. S. (2003). Importance of vertical geochemical processes in controlling the oceanic profiles of dissolved rare earth elements in the northeastern Indian Ocean. *Earth and Planetary Science Letters*, *205*, 155–172. https://doi.org/10.1016/S0012-821X(02)01027-0

Nozaki, Y., Horibe, Y., & Tsubota, H. (1981). The water column distributions of thorium isotopes in the western North Pacific. *Earth and Planetary Science Letters*, *54*(2), 203–216. https://doi.org/10.1016/0012-821X(81)90004-2

Orians, K. J., & Bruland, K. W. (1986). The biogeochemistry of aluminum in the Pacific Ocean. *Earth and Planetary Science Letters*, *78*(4), 397–410. https://doi.org/10.1016/0012-821X(86)90006-3

Powell, C. F., Baker, A. R., Jickells, T. D., Bange, H. W., Chance, R. J., & Yodle, C. (2015). Estimation of the atmospheric flux of nutrients and trace metals to the eastern tropical North Atlantic Ocean. *Journal of the Atmospheric Sciences*, *72*(10), 4029–4045. https://doi.org/10.1175/JAS-D-15-0011.1

Prospero, J. M. (1996). Saharan dust transport over the North Atlantic Ocean and Mediterranean: An overview. In S. Guerzoni, & R. Chester (Eds.), The impact of desert dust across the Mediterranean (Vol. 11, pp. 133–151). Springer Netherlands. https://doi.org/10.1007/978-94-017-3354-0_13

Prospero, J. M., & Carlson, T. N. (1972). Vertical and areal distribution of Saharan dust over the western equatorial north Atlantic Ocean. *Journal of Geophysical Research*, *77*(27), 5255–5265. https://doi.org/10.1029/JC077i027p05255

Prospero, J. M., Collard, F.-X., Molinié, J., & Jeannot, A. (2014). Characterizing the annual cycle of African dust transport to the Caribbean Basin and South America and its impact on the environment and air quality. *Global Biogeochemical Cycles*, *28*(7), 757–773. https://doi.org/10.1002/2013GB004802

Rad, S., Louvat, P., Gorge, C., Gaillardet, J., & Allègre, C. J. (2006). River dissolved and solid loads in the Lesser Antilles: New insight into basalt weathering processes. *Journal of Geochemical Exploration*, *88*(1–3), 308–312. https://doi.org/10.1016/j.gexplo.2005.08.063

Rad, S., Rivé, K., Vittecoq, B., Cerdan, O., & Allègre, C. J. (2013). Chemical weathering and erosion rates in the Lesser Antilles: An overview in Guadeloupe, Martinique and Dominica. *Journal of South American Earth Sciences*, *45*, 331–344. https://doi.org/10.1016/j.jsames.2013.03.004

Radic, A., Lacan, F., & Murray, J. W. (2011). Iron isotopes in the seawater of the equatorial Pacific Ocean: New constraints for the oceanic iron cycle. *Earth and Planetary Science Letters*, *306*, 1–10. https://doi.org/10.1016/j.epsl.2011.03.015

Resing, J. A., & Measures, C. I. (1994). Fluorometric determination of Al in seawater by flow injection analysis with in-line preconcentration. *Analytical Chemistry*, *66*(22), 4105–4111. https://doi.org/10.1021/ac00094a039

Resing, J. A., Sedwick, P. N., German, C. R., Jenkins, W. J., Moffett, J. W., Sohst, B. M., & Tagliabue, A. (2015). Basin-scale transport of hydrothermal dissolved metals across the South Pacific Ocean. *Nature*, *523*(7559), 200–203. https://doi.org/10.1038/nature14577

Richardson, P. L., & Walsh, D. (1986). Mapping climatological seasonal variations of surface currents in the tropical Atlantic using ship drifts. *Journal of Geophysical Research*, *91*(C9), 10537. https://doi.org/10.1029/JC091iC09p10537

Rijkenberg, M. J. A., Middag, R., Laan, P., Gerringa, L. J. A., van Aken, H. M., Schoemann, V., et al. (2014). The distribution of dissolved iron in the West Atlantic Ocean. *PLoS One*, *9*(6), e101323. https://doi.org/10.1371/journal.pone.0101323

Roy-Barman, M., & Jeandel, C. (2016). *Marine geochemistry : Ocean circulation, carbon cycle and climate change*. Oxford University Press. https://doi.org/10.1093/acprof:oso/9780198787495.001.0001

Rudnick, R. L., & Gao, S. (2014). Composition of the continental crust. In *Treatise on geochemistry* (pp. 1–51). Elsevier. https://doi.org/10.1016/B978-0-08-095975-7.00301-6

Schlitzer, R., Anderson, R. F., Dodas, E. M., Lohan, M., Geibert, W., Tagliabue, A., et al. (2018). The GEOTRACES intermediate data product 2017. *Chemical Geology*, *493*, 210–223. https://doi.org/10.1016/j.chemgeo.2018.05.040

Shelley, R. U., Landing, W. M., Ussher, S. J., Planquette, H., & Sarthou, G. (2018). Regional trends in the fractional solubility of Fe and other metals from North Atlantic aerosols (GEOTRACES cruises GA01 and GA03) following a two-stage leach. *Biogeosciences*, *15*(8), 2271–2288. https://doi.org/10.5194/bg-15-2271-2018

Stoffyn, M. (1979). Biological control of dissolved aluminum in seawater: Experimental evidence. *Science*, *203*(4381), 651–653. https://doi.org/10.1126/science.203.4381.651

Stoffyn, M., & Mackenzie, F. T. (1982). Fate of dissolved aluminum in the oceans. *Marine Chemistry*, *11*(2), 105–127. https://doi.org/10.1016/0304-4203(82)90036-6

Tria, J., Butler, E. C. V., Haddad, P. R., & Bowie, A. R. (2007). Determination of aluminium in natural water samples. *Analytica Chimica Acta*, *588*(2), 153–165. https://doi.org/10.1016/j.aca.2007.02.048

van Hulten, M. M. P., Sterl, A., Tagliabue, A., Dutay, J.-C., Gehlen, M., de Baar, H. J. W., & Middag, R. (2013). Aluminium in an ocean general circulation model compared with the West Atlantic Geotraces cruises. *Journal of Marine Systems*, *126*, 3–23. https://doi.org/10.1016/j.jmarsys.2012.05.005

Viers, J., Dupré, B., & Gaillardet, J. (2009). Chemical composition of suspended sediments in World Rivers: New insights from a new database. *The Science of the Total Environment*, *407*(2), 853–868. https://doi.org/10.1016/j.scitotenv.2008.09.053

Wagener, T., Guieu, C., & Leblond, N. (2010). Effects of dust deposition on iron cycle in the surface Mediterranean Sea. *Biogeosciences Discussions*, 2799–2830.

Weber, T., John, S., Tagliabue, A., & DeVries, T. (2018). Biological uptake and reversible scavenging of zinc in the global ocean. *Science*, *361*(6397), 72–76. https://doi.org/10.1126/science.aap8532

Wuttig, K., Wagener, T., Bressac, M., Dammshäuser, A., Streu, P., Guieu, C., & Croot, P. L. (2013). Impacts of dust deposition on dissolved trace metal concentrations (Mn, Al and Fe) during a mesocosm experiment. *Biogeosciences*, *10*(4), 2583–2600. https://doi.org/10.5194/bg-10-2583-2013

Ye, Y., Wagener, T., Völker, C., Guieu, C., & Wolf-Gladrow, D. A. (2011). Dust deposition: Iron source or sink? A case study. *Biogeosciences*, *8*(8), 2107–2124. https://doi.org/10.5194/bg-8-2107-2011